DOE/NASA/1040-78/30
NASA TM-79044

INITIAL COMPARISON OF SINGLE CYLINDER STIRLING ENGINE COMPUTER MODEL PREDICTIONS WITH TEST RESULTS

Roy C. Tew, Jr., Lanny G. Thieme,
and David Miao
National Aeronautics and Space Administration
Lewis Research Center

Work performed for
U. S. DEPARTMENT OF ENERGY
Office of Conservation and Solar Applications
Division of Transportation Energy Conservation

TECHNICAL PAPER to be presented at the
International Congress and Exposition
sponsored by the Society of Automotive Engineers
Detroit, Michigan, February 26 - March 4, 1979

DOE/NASA/1040-78/30
NASA TM-79044

INITIAL COMPARISON OF SINGLE CYLINDER STIRLING ENGINE COMPUTER MODEL PREDICTIONS WITH TEST RESULTS

Roy C. Tew, Jr., Lanny G. Thieme,
and David Miao
Lewis Research Center
Cleveland, Ohio 44135

Prepared for
U. S. DEPARTMENT OF ENERGY
Office of Conservation and Solar Applications
Division of Transportation Energy Conservation
Washington, D. C. 20545
Under Interagency Agreement EC-77-A-31-1040

International Congress and Exposition
sponsored by the Society of Automotive Engineers
Detroit, Michigan, February 26-March 4, 1979

THE WORK REPORTED ON HEREIN was performed in support of the U.S. Department of Energy (DOE) Stirling Engine Highway Vehicle System Program for which the Lewis Research Center (LeRC), through an Interagency agreement with DOE, has project management responsibility under the programmatic direction of the DOE Division of Transportation Energy Conservation.

One objective of this program is to make validated Stirling engine performance and design optimization computer codes available to all who wish to do research and development work on Stirling engines. Although private industry has been given contractual responsibility for the code development, NASA Lewis has been developing a performance code and attempting to validate it against experimental data. This approach makes it possible for us to contribute directly toward the development of validated codes and to manage the contractual code development more intelligently.

One version of the code which models the engine of a rhombic-drive ground power unit (GPU) has already been reported in reference (1).* This paper updates that model and compares its predictions with recent GPU test results.

This test GPU was designed and built for the Army by General Motors. The unit was designed to produce 3 kW of electric power.

GENERAL DESCRIPTION OF MODEL

The GPU engine, for which this model predicts performance, is shown schematically in Fig. 1. The engine incorporates eight regenerator/cooler units. The model assumes that identical flow conditions exist in each of these eight parallel flow paths. The model represents the working space by a series of subdivisions called control volumes; this type of model is sometimes called a nodal model.

The engine working space is represented by 13 control volumes, as shown in Fig. 2; the adjacent metal walls are represented by 13 corresponding control volumes. The metal temperatures, except for those in the regenerator, are assumed to be constant. This is a reasonable assumption for any given run since the heater and cooler metal temperatures

---

*Numbers in parentheses designate References at end of paper.

are essentially boundary temperatures that are controlled by the combustor and the cooling water flow, respectively; these temperatures vary little over a cycle because the metal heat capacity is much greater than that of the gas. The appropriate fixed cooler metal temperatures are determined from cooling water inlet temperature, flow rate and the calculated heat rejection per cycle (this requires several iterations since heat rejection is a function of the cooler tube temperature); compression space metal temperature was assumed equal to the cooler metal temperatures.

The model calculates indicated power and efficiency for a given engine speed, mean pressure, heater and expansion space metal temperatures, and cooler water inlet temperature and flow rate. The indicated efficiency is based on heat into the gas plus conduction losses. The model also simulates temperature, pressure, and flow variations over the cycle at various stations in the working space.

The present model incorporates engine mechanical losses, as calculated from heat balances measured during the recent LeRC GPU tests.

The thermodynamic equations and assumptions used in developing the model were reported in reference 1. The modifications which have been made to the model since publication of reference 1 are discussed in the appendix to this paper.

The calculation procedure used in the model is outlined in Fig. 3. Each set of calculations, indicated in Fig. 3 within the inner loop (except for pressure-drop, conduction, and shuttle losses), is made at each integration time step during each cycle. It is necessary to make the pressure drop calculations only over the last cycle since, as explained in reference 1, the pressure drop calculations are decoupled from the heat and mass transfer calculations. Conduction and shuttle losses are calculated just once during the last cycle.((Shuttle heat transfer occurs by heating of the displacer at the hot end of the stroke and cooling at the cold end of the stroke (2).) The regenerator metal temperature convergence scheme (1) was turned on after the 5th cycle, and off after the 25th cycle. During this time, the regenerator metal temperatures were corrected after each cycle and the cooler tube temperatures were corrected after every 4th cycle. With the temperatures converged, the calculations proceed through five more cycles to allow further settling out and the run is terminated with the completion of the 30th cycle.

The computer program is written in FORTRAN V and, in card format, is about 1300 cards long (including plotting subroutines). Current computing time is about 3.75 minutes for 30 cycles on a UNIVAC 1100, or 0.125 minute per cycle. This is based on 1000 iterations per cycle (which implies a time increment of 2×10^{-5} sec when the engine frequency is 50 Hz).

The computing time can be decreased by decreasing the number of iterations per cycle; the corresponding effect on predicted indicated power and efficiency is shown in Figs. 4 and 5 for one series of runs of an earlier version of the model. These figures show that some error was introduced by reducing from 1000 to 500 iterations per cycle and that the error became more significant if only 200 iterations per cycle were used.

COMPARISON WITH OTHER MODELS

The model described herein is less general than the models of Urieli (3,4), Shock (5), and Finegold and Vanderbrug (6) in that it neglects the effects of gas inertia (and pressure-wave dynamics) and gas kinetic energy. By neglecting these effects it is possible to use an integration technique which allows a trade-off between computing time and accuracy of solution without concern for numerical instability and which results in a savings of computer time.

Urieli has used his model to predict the performance of one prototype engine for which the above mentioned effects appear to be very significant at 50 Hz operating speed (7). However, these effects were assumed to be negligible in the GPU (maximum Mach numbers were calculated to be about 0.05 for hydrogen and 0.075 for helium at design spedd and pressure level (50 Hz, 6.90 10^6 N/m^2 or 3000 rpm, 1000 psi)).

The LeRC model differs from the Rios (8) and the Martini (2,9) models in that in more closely represents the "distributed parameter" nature of the working space by dividing each heat exchanger into several control volumes and making the heat exchanger inefficiencies an integral part of the cycle calculations.

The Lewis model is thus more general but less efficient, in terms of computing time, than the models of Rios and Martini.

Neither the LeRC or any one of the more general models (i.e., those of Urieli, Shock, and Finegold and Vanderbrug) would be suitable for a design optimization program because of excessive computing time. One run of a Stirling engine design optimization program may require the prediction of engine performance at several thousand different configurations and/or operating conditions. Of the models mentioned here only the Martini or Rios models appear to be sufficiently efficient in terms of computing time to serve as the basis for an optimization code.

ENGINE DESCRIPTION AND BACKGROUND

The GPU-3 (Ground Power Unit) was obtained from the U.S. Army Mobility Equipment Research and Development Center (MERDC) at Fort Belvoir, Virginia. It was designed and built by the General Motors Research Laboratories in 1965 for the U.S. Army. The progress reports on the development of the engine and its components by General Motors as well as other useful information concerning the GPU are given in reference 10.

The GPU-3 engine is a single-cylinder displacer-type engine with rhombic drive and sliding rod seals. It is capable of producing a maximum engine output of approximately 7.5 kW (10 hp) with hydrogen working fluid at 6.9×10^6 N/m^2 (1000 psi) mean compression-space pressure. The piston swept volume is 120 cc (7.3 in^3).

The engine obtained from Fort Belvoir was initially torn down and restored to operating condition. It was then tested as part of the original GPU-3 package with only those changes made that were necessary to make the unit operable. Those results and a description of the engine hardware are given in reference 11.

To obtain the data necessary for comparison to the computer simulation, the engine was modified as follows:

(1) The engine-driven accessories from the original GPU-3 package were removed with the exception of the lubrication oil system.

(2) Air, water, fuel, and working fluid were provided from the facility support systems.

(3) Instrumentation was added to obtain an energy balance, engine temperature profiles, working space gas temperatures, dynamic pressures, and to measure indicated work.

The original GPU-3 alternator and a separate resistance load bank were used to absorb the engine output power. The alternator was calibrated to define its efficiency at various speeds and output voltages. Since the GPU-3 package was designed for a 3-kW output, the alternator was not capable of absorbing the maximum output power of the engine.

Engine dimensions and parameters needed in the simulation were determined and are given in Table 1. A breakdown of the engine dead volume as calculated from hardware measurements is given in Table 2 together with the measured value of minimum working space volume (obtained by a gas displacement method). The calculated value of minimum working space volume is seen to be within 2 percent of the measured value.

The GPU-engine is shown schematically in Fig. 1. A more accurate schematic of the top portion of the engine (which shows the dimensions needed for heat conduction calculations) is shown in Fig. 6. The geometric relations between piston positions and crankshaft angle are shown schematically in Fig. 7. Equations for calculating compression-, expansion-, and buffer-space volumes are given in reference 1.

PREDICTION PROCEDURE - The following procedure was used in setting the model up to make comparisons with the experimental data:

Heater tube and expansion space metal temperatures were set to average values of the corresponding measured metal temperatures. Measured temperature profiles in the cylinder, regenerator, and insulation container (which encloses the insulation packed around the regenerators) were input to the model for use in conduction calculations. Measured water temperature into the cooler and water flow rate were used together with the calculated heat out to estimate the average cooler tube temperature (this required several iterations).

The reference heat transfer and pressure drop co relations identified in the appendix were used. However, the regenerator friction factor was adjusted to give best agreement between predicted and experimental indicated powers. (This will be discussed further in the next section.)

The experimentally determined mechanical losses, discussed in the appendix, were used to determine predicted brake power from predicted indicated power.

With the above procedure it was found that the time averaged predicted gas temperatures were lower in the heater and higher in the cooler than the corresponding measured gas temperatures. Good agreement between predicted and experimental average gas temperatures could be obtained by increasing the model heat transfer coefficients in the heater and cooler. But increasing these coefficients made the agreement between predicted and experimental engine power and efficiency worse. Therefore, for these runs, we did not attempt to bring the predicted and experimental gas temperatures into close agreement.

An optional procedure, which has been considered but not yet tried, would be to assume that the measured heater gas temperature is correct and to set the model heater metal temperatures to the values required to match the measured gas temperature. At this time it is not clear which of the two sets of temperature measurements (metal or gas) is the more correct.

COMPARISON OF MODEL PERFORMANCE PREDICTION WITH EXPERIMENTAL DATA

Baseline tests were run to map the engine performance over a range of heater gas temperatures from 595° to 705° C (1100° to 1300° F), mean compression-space pressures of 1.4 to 6.9×10^{6} N/m^{2} (200 to 1000 psi), and engine speeds from 1000 to 3500 rpm with both hydrogen and helium as the working fluids. These experimental results are reported in reference 12.

Comparison of experimental and predicted indicated powers suggested that the engine pressure drop was underestimated when the reference set of friction factors and end effects were used in the model. (The end effects calculations are described in ref. 1.) Since the regenerator accounts for most of the calculated frictional pressure drop, the regenerator friction factor was adjusted to get better agreement between predictions and data. For runs made with hydrogen working gas the plot of indicated power shown in Fig. 8 suggests that predicted indicated power agrees best with the test data if four times the reference regenerator friction factor is used; this factor of 4 produced the best overall agreement for all test points made with hydrogen working gas.

The reference regenerator and cooler friction factors are based on steady-flow air tests that were made on the newly manufactured regenerator-cooler units prior to the engine tests. Examination of the regenerator-cooler units after the engine tests revealed they had been contaminated with oil. Steady flow air tests of the oil contaminated components (i.e., tests on (1) the complete heater head-regenerator-cooler flow system and (2) three individual regenerator-cooler units) were completed after the computer predictions discussed in this paper were completed. Preliminary analysis of these results indicate that the three contaminated regenerator-cooler components have about one-third greater pressure drop than when clean and also the spread in pressure drop from one unit to another has increased. Also the flow tests on the complete heater head, regenerator, cooler flow system suggest that the pressure drop due to end effects appears almost as large as the regenerator frictional pressure drop. It thus appears that loss due to end effects is being underestimated in the computer model. Further analysis using these airflow results will be required before the appropriate modifications can be made to the computer model.

Other possible explanations for additional pressure drop are:

(1) Increased pressure drop due to methane (which can be produced by thermal cracking of the oil contaminant). In reference 13 (p. 9) it is stated that in the General Motor tests "the effect [of methane production] was much more significant than had ever been noted by plugging of the heat exchangers by solid residue." In future tests it is planned to periodically analyze samples of the working gas to evaluate the effect of such impurities.

(2) Error due to use of steady flow friction factor correlations to predict pressure drop for periodically reversing flow.

(3) Errors in pressure drop prediction due to the neglect of gas inertia and gas kinetic energy. (These effects are probably not significant in the GPU at the low Mach numbers encountered (< 0.1) when hydrogen

and helium are used at speeds at or below 3500 rpm.)

Another possibility is that we may be underestimating the true mechanical loss; such an error would make the apparent pressure drop loss appear larger (see the discussion of mechanical loss in the appendix).

Performance predictions are compared with the experimental results for hydrogen working gas in Figs. 9 to 12; four times the reference regenerator friction factor was used in the model to make all predictions shown in these figures. Brake power is shown as a function of engine speed for several pressure levels in Fig. 9. The 4.14×10^6 N/m^2 (600 psi) pressure was the highest experimental pressure that could be achieved without overloading the alternator; the alternator limitation also prevented completion of the experimental curve at this highest pressure level (see Fig. 9). Agreement is within 6 percent of the experimental values at the 2.76×10^6 N/m^2 (400 psi) and 4.14×10^6 N/m^2 (600 psi) pressures. At the 1.38×10^6 N/m^2 (200 psi) mean pressure level although the absolute error in predicted power is no greater than 0.22 kW (0.3 hp) the percentage error is as high as 44 percent due to the low power level.

Predicted and experimental brake efficiencies are compared in Fig. 10 for the same hydrogen runs. Brake efficiency is defined as follows:

$$\text{Brake efficiency} = \frac{\text{brake power}}{\text{rate of heat input to engine}}$$

Two sets of experimental brake efficiencies are shown for each pressure level. Results of two methods of determining the experimental heat input rate, used in determining these two sets of experimental brake efficiencies, are compared with the predicted heat input rate in Fig. 11. One set of values was determined by a hot end energy balance as follows:

$$\text{Heat input rate}\Big|_{\text{hot end energy balance}} = \text{heat produced by fuel} - [\text{sum of heat loss rates via exhaust gas, fuel nozzle cooling water, conduction, and radiation}]$$

This set of heat input values was the higher and therefore gave the lower experimental efficiencies. Complete combustion of the fuel was assumed. The lower heat input values in Fig. 11, which correspond to the higher experimental efficiencies in Fig. 12, were determined as follows:

$$\text{Heat input rate}\Big|_{\text{cold end energy balance}}$$

$$= \text{brake power} + [\text{sum of heat rejection via the cooling water and oil}]$$

In Fig. 10 the predicted value of efficiency at 4.14×10^6 N/m^2 (600 psi) is 7 percent above the upper experimental value. At 2.76×10^6 N/m^2 (400 psi) the predicted values of efficiency range from 6 to 16 percent above the upper experimental values with best agreement at the higher speeds where power and heat input are largest. At 1.38×10^6 N/m^2 (200 psi) there is a large spread between the two sets of experimental values indicating a high degree of uncertainty. This is probably due to the fact that the errors in estimating various losses (radiation, convection, exhaust losses, etc.) represent a larger percentage of the brake power and heat input to the engine than at higher pressure levels. The predicted values of efficiency range from 6 to 30 percent above the upper set of experimental values at this mean pressure with best agreement again at the higher speeds.

In Fig. 11 the difference between experimental and predicted values of heat input may be attributable in part to lowered experimental regenerator effectiveness (and therefore higher heat input) due to oil contamination. At 4.14×10^6 N/m^2 (600 psi) the predicted heat input is about 3 percent below the lower experimental value. At 2.76×10^6 N/m^2 (400 psi) the predicted heat input is about 0.45 kW (0.6 hp) lower over the whole range. At 1.38×10^6 N/m^2 (200 psi) the predicted heat input is within the range of the experimental values except in the low speed range where it falls slightly below the lower experimental values.

The effect of different heater gas temperatures on the comparison of predicted and experimental brake powers is shown in Fig. 12 for hydrogen working gas at 2.76×10^6 N/m^2 (400 psi). The comparison suggests that the model accurately predicted the effects of changes in heater gas temperature on brake power. Correlation of predicted and experimental values of brake efficiency and heat input for 649° C (1200° F) and 593° C (1100° F) were not significantly different than for the 704° C (1300° F) heater gas temperature.

For helium working gas, comparisons of predicted and experimental indicated power such as that shown in Fig. 13 show that best agreement with the test data results when about 2.6 times the reference generator friction factor is used. Although the comparison is shown for 2.76×10^6 N/m^2 (400 psi) mean pressure and 704° C (1300° F) heater gas temperature, the choice of the factor of 2.6 was based on such comparisons over the mean pressure range from 2.76×10^6 N/m^2 (400 psi) to 6.90×10^6 N/m^2 (1000 psi) at 649° C (1200° F) heater gas temperature.

Theoretically the same friction factor - Reynolds number correlations and end effects calculations should apply to both hydrogen and helium. The fact that different "correction factors" for regenerator friction factor were required to get best agreement with the data may be due in part to the following:

(1) The hydrogen tests were made after the helium tests; thus the larger friction factor required to fit the hydrogen data may be due in part to additional solid residue from oil that was deposited after completion of the helium tests.

(2) Also any methane produced by breakdown of the oil would cause a larger percentage error in the pressure drop calculation for the hydrogen than for the helium runs (since methane is closer in density to helium than to hydrogen).

(3) It is shown in the appendix that the experimentally determined mechanical losses were higher for helium than for hydrogen. This result is supported by results discussed briefly in reference 10 (Sec. 1.206, p. 4). If, however, the results shown in the appendix overestimate the difference between helium and hydrogen mechanical losses, an effect would be to cause an apparent difference between friction factors for hydrogen and helium such as that already noted.

Performance comparisons for helium working gas are shown in Figs. 14 to 18; 2.6 times the reference regenerator friction factor was used in the model to make all predictions shown in these figures. In the brake power plot of Fig. 14 (for 649° C (1200° F) heater temperature) the predicted power ranges from 2 to 15 percent above the experimental power for all points except the one of lowest power.

The corresponding brake efficiencies are compared in Fig. 15. In Fig. 15(a) the predicted efficiencies range from 3 to 17 percent above the upper experimental values at all points except the point of lowest efficiency.

In Fig. 15(b) for 5.52×10^6 N/m^2 (800 psi) the predicted values lie above the upper experimental values by from 10 to 15 percent over the range tested. In Fig. 15(c) for 6.90×10^6 N/m^2 (1000 psi) the predicted values exceed the upper experimental values by about 12 percent over the range tested.

The corresponding values of heat in are compared in Fig. 16. At 6.90×10^6 N/m^2 (1000 psi) and 5.52×10^6 N/m^2 (800 psi) the predicted values lie within the range of experimental values. For 4.14×10^6 N/m^2 (600 psi) and 2.76×10^6 N/m^2 (400 psi) the predicted heat in is slightly low at the higher engine speeds but still within 4 percent of the lower experimental values. Thus errors in predicted brake efficiency for this set of helium runs are primarily due to overprediction of power.

Predicted and experimental brake powers for 704° C (1300° F) nominal heater gas temperature are compared in Fig. 17. The shapes of the predicted curves are in good agreement with the data; however, the magnitudes are more optimistic than for those runs made at 649° C (1200° F) nominal heater gas temperature. At 5.52×10^6 N/m^2 (800 psi) the predicted values are within 10 percent of the experimental values. However at 4.14×10^6 N/m^2 (600 psi) and 2.76×10^6 N/m^2 (400 psi) the predicted values range from 19 to 28 percent and from 7 to 34 percent, respectively, above the experimental values. Correlation between predicted and experimental power at 4.14×10^6 N/m^2 (600 psi) is notably worse than for the corresponding 649° C (1200° F) case shown in Fig. 14. At 1.38×10^6 N/m^2 (200 psi), the maximum absolute error is 0.15 kW (0.2 hp) over the range tested.

Predicted and experimental brake powers for 593° C (1100° F) nominal heater gas temperature are compared in Fig. 18.

SUMMARY

This paper compares predictions of an updated version of the LeRC GPU Stirling engine computer model (1) with recent GPU tests performed at LeRC.

Comparisons of predicted and experimental indicated powers implied that the reference pressure drop calculations were underestimating actual engine pressure drop. This result seemed consistent with (1) the presence of oil contamination in the regenerator-cooler units after engine testing, (2) preliminary analysis of flow tests on the entire flow system and on several of the oil contaminated regenerator-cooler units, and (3) the possible presence of methane in the working gas due to thermal cracking of oil.

Another possibility is that the LeRC mechanical loss data may underestimate the true mechanical loss; such an error would make the apparent pressure drop loss, as implied by experimental indicated power, appear larger.

The procedure used in this comparison was to adjust the regenerator friction factor to give best agreement between predicted and indicated powers. For hydrogen working gas a factor of 4 times the reference regenerator friction gave best results and for helium a factor of about 2.6 was best. This apparent difference in friction factors for hydrogen and helium, although theoretically unreasonable, would be consistent with (1) progressive accumulation of solid residue from oil contamination (the hydrogen tests were done after the helium tests) and (2) possible presence of methane (which would affect the hydrogen results more than the helium. Any overestimate of the true difference between helium and hydrogen mechanical losses would also tend to produce an apparent difference in helium and hydrogen friction factors such as that noted above.

Results of the comparisons between predicted and experimental brake power and efficiency are summarized in Table 3; the predictions were made using the adjustments in regenerator friction factor discussed above. Table 3 shows that for hydrogen working gas the predicted values of brake power ranged from 0 to 6 percent above the experimental values at the two higher pressure levels. For the corresponding predicted brake effi-

ciencies the error range was higher (from 6 to 16 percent above the upper set of experimental brake efficiencies). In general the highest percentage errors occurred at the low power and efficiency points. For helium with 649° C (1200° F) heater gas temperature the predicted brake power was 2 to 15 percent greater than the experimental (except for one point) over a wider pressure range than could be covered with hydrogen working gas; the percent error range for the corresponding predicted brake efficiencies was about the same as for brake power. The correlation between predicted and experimental brake powers is seen, in Table 3, to be worse for helium at 704° C (1300° F) heater gas temperature than at 649° C (1200° F).

Due to uncertainties in the various true losses - pressure drop, mechanical loss, leakage, heat exchanger inefficiencies, etc. - it is possible to obtain good performance predictions for a given set of engine tests with a combination of incorrect loss predictions. Thus individual losses are better determined by special tests and/or instrumentation rather than implied by overall results. Therefore attempts must be made to obtain better definition of the various losses. The recent flow tests on the oil contaminated components imply that pressure drop loss due to end effects and oil contamination has not been properly accounted for in the model. Periodic samples of the working gas must be made to determine if significant amounts of methane or other contaminants are present. Motoring tests of the engine will be made and an attempt will be made to improve the direct measurement of indicated power to develop more confidence in the mechanical loss definition. It may be possible to improve the leakage loss estimate by use of techniques discussed in reference 10 (Sec. 5).

It should be noted that only one of the test points discussed in this paper was taken at the design operating pressure of 6.90×10^{6} N/m^2 (1000 psi). It may be unreasonable to expect great accuracy at pressures as low as 1.38×10^{6} N/m^2 (200 psi) when several tenths of a kilowatt can lead to such large percentage errors. The next series of tests with the engine on a dynamometer should result in complete maps of engine performance for use in model validation.

APPLNDIX - MODEL UPDATES SINCE PUBLICATION OF REFERENCE 1

1. CALCULATION OF COOLER TUBE TEMPERATURE - When the Model was reported in reference 1 it was assumed that the water side heat transfer coefficient in the cooler was so large compared to the gas side coefficient that the cooler tube temperature was essentially at the average water temperature. Information given in reference 10 suggests that the above assumption was a poor one. Consequently, cooler tube temperature is now calculated as follows:

The heat transfer correlation used on the water side is

$$\frac{h_w D}{k} = 0.35\ N_{Re}^{0.55} N_{PR}^{0.33} \qquad (1)$$

(from (15)) where

h_w water side heat transfer coefficient

D hydraulic diameter (heater tube outside diameter)

k water thermal conductivity

N_{RE} Reynolds number

N_{PR} Prandtl number

In addition a fouling factor F, of 0.882 m^2-^oC/kW (0.005 hr-ft^2-^oR/Btu) is assumed to exist on the water side. Thus the total coefficient on the water side is:

$$h_t = \frac{1}{\frac{1}{h_w} + F}$$

Thus if h_w = 1.134 kW/m^2-^oC (2000 Btu/hr-ft^2-^oR) then

$$h_t = \frac{1}{\frac{1}{1.134} + 0.882} = 0.567\ \text{kW/m}^2\text{-}^o\text{C}$$

(1000 Btu/hr-ft^2-^oR)

The fouling factor, in this case, cuts the water side coefficient in half. In calculating the water side Reynolds number

$$N_{Re} = \frac{GD}{\mu}$$

the flow per unit area G, is based on an effective flow area of 3.01 cm^2 (0.467 in^2) for the total cooler water flow (one-half of the cooler water flow passes through each cooler).

The equation used to calculate tube temperature from the inlet water temperature is

$$T_{tube} = T_{w_{in}} + Q_{out}\left[\frac{1}{2C_{PW}W_w} + \frac{\ln(r_o/r_i)}{2\pi Lk_m} + \frac{1}{h_tA_w}\right] \quad (2)$$

where

Q_{out}	heat out of engine over one cycle
C_{PW}	specific heat of water
W_w	water flow rate
r_o, r_i	outside and inside radii of cooler tube
L	total heat transfer length of cooler tubes
k_m	thermal conductivity of cooler tube
h_t	total heat transfer coefficient, water side
A_w	total heat transfer area on water side

Since the value of Q_{out} is changing from cycle to cycle during the convergence procedure it is necessary to repeat this calculation several times. The correction is made after every 4th cycle during the sequence of cycles when the regenerator metal temperatures are being corrected after each complete cycle.

The portion of the heat rejection due to pressure loss was neglected in determining the temperature difference between the cooler wall and the cooling water. This caused an overprediction of power estimated to be no more than 2 to 3 percent (with the largest errors occurring with helium working gas at the highest engine speed).

2. LEAKAGE LOSS - The simplified equations incorporated in the model for calculating leakage throughout the cycle, described in reference 1, were not used for this set of runs. These equations always give the same mean pressure for working and

buffer spaces. The test data showed that this assumption is not a good one.

Instead an estimate of the power loss due to leakage between working and buffer spaces was made based on information given in reference 10 (Sec. 6.006). According to this information the power loss due to leakage is about 0.45 kW (0.6 hp) for hydrogen working gas at the design mean pressure of 6.90×10^6 N/m^2 (1000 psi). An equation derived in this reference for power loss due to leakage between working and buffer spaces implies that this power loss is proportional to the square of the mean pressure level and is independent of engine speed. The equation also indicates that this leakage power loss is inversely proportional to the square root of the molecular weight. Using these relationships and assuming that the 0.45 kW (0.6 hp) leakage loss for hydrogen is due only to leakage between working and buffer spaces, the leakage losses in Table 4 were generated and used in the model.

3. MECHANICAL LOSS - Mechanical loss curves for hydrogen and helium are shown in Figs. 19 and 20. At the 4.14×10^6 N/m^2 (600 psi), 58.33 Hz (3500 rpm) point the mechanical loss with helium working gas is about 19 percent greater than with hydrogen. At 2.76×10^6 N/m^2 (400 psi) mean pressure the mechanical loss with helium is higher than with hydrogen by from 9 percent at 16.67 Hz (1000 rpm) to 26 percent at 58.33 Hz (3500 rpm). At 1.38×10^6 N/m^2 (200 psi) the mechanical loss with helium ranges from 7 to 42 percent higher than with hydrogen over the speed range tested.

These mechanical loss curves were determined from experimental heat balances taken during the recent LeRC GPU tests. It was assumed that the sum of the heat to the buffer space cooling water and to the oil equaled the mechanical loss. According to reference 10 (Sec. 6.006) General Motors concluded that this heat balance approach to estimating mechanical loss was probably more accurate than use of motoring loss data.

The mechanical loss for hydrogen at 2.76×10^6 N/m^2 (400 psi), from Fig. 19, can be compared to General Motors motoring loss data (10) (Sec. 6.006, p. 36); at 3000 rpm the motoring loss data, which includes leakage, implies a loss about 0.37 kW (0.5 hp) greater than the mechanical loss data of Fig. 19. Table 4 shows a leakage loss of

0.07 kW (0.10 hp) for hydrogen at 2.76×10^6 N/m^2 (400 psi).

The implication of the above is that the LeRC mechanical loss data indicates about 0.3 kW (0.4 hp) less mechanical loss (at 3000 rpm and 2.76×10^6 N/m^2 (400 psi)) than the General Motors motoring loss data. The difference between the mechanical losses predicted by the two sets of data decreases linearly with speed until they agree at approximately 1600 rpm.

The relative difference between the helium and hydrogen mechanical losses (Figs. 19 and 20) agrees well with information given in reference 10 (Sec. 1.206, p. 4) for 3000 rpm and 4.83×10^6 N/m^2 (700 psi).

4. HEAT TRANSFER CORRELATIONS - Steady-flow heat transfer correlations from reference 14 are used in the heater and cooler (Fig. 7-1, p. 123 of ref. 14) and the regenerator (Fig. 7-8, p. 129 of ref. 14). The validity of these correlations is more widely accepted than the ones used in the model when it was reported on in reference 1.

5. FRICTION FACTOR CORRELATIONS - Curves of friction factor, f, as a function of Reynolds number, N_{Re}, were derived from NASA Lewis steady-flow air data for the regenerators and coolers; these curves are shown in Figs. 21 and 22. The regenerator Reynolds number is based on hydraulic diameter (rather than wire diameter). The friction factor correlation used in the heater is a standard one from reference 15; the form of this correlation used in the model is:

$$f = 16/N_{Re} \qquad N_{Re} < 1500$$

$$f = 0.046/N_{Re}^{0.2} \qquad N_{Re} \geq 1500$$

This correlation was not satisfactory for use in the cooler because the small cooler tube diameter implies a large relative roughness.

REFERENCES

1. R. Tew, K. Jefferies, and D. Miao, "A Stirling Engine Computer Model for Performance Calculations," DOE/NASA/1011-78/24, NASA TM-78884, July 1978.

2. W. R. Martini, "Stirling Engine Design Manual," Washington University, Wash., NASA Grant NSG-3152. NASA CR-135382, 1978.

3. I. Urieli, C. J. Rallis, and D. M. Berchowitz, "Computer Simulation of Stirling Cycle Machines," Twelfth Intersociety Energy Conversion Engineering Conference Proceedings, Vol. 2. LaGrange Park, Ill., American Nuclear Society, Inc., 1977, pp. 1512-1521.

4. I. Urieli, "A Computer Simulation of Stirling Cycle Machines," Ph.D. Thesis, University Witwatersrand, Johannesburg, South Africa, 1977.

5. A. Schock, "Nodal Analysis of Stirling Cycle Devices," Thirteenth Intersociety Energy Conversion Engineering Conference Proceedings, Vol. 3. Warrendale, Pa., Society of Automotive Engineers, Inc., 1978, pp. 1771-1779.

6. J. G. Finegold, and T. G. Vanderbrug, "Stirling Engines for Undersea Vehicles," JPL Report 5030-63, Jet Propulsion Lab., 1977.

7. I. Urieli, "A Computer Simulation of the JPL Stirling Laboratory Research Engine," Thirteenth Intersociety Energy Conversion Engineering Conference Proceedings, Vol. 3. Warrendale, Pa., Society of Automotive Engineers, Inc., 1978, pp. 1780-1783.

8. P. A. Rios y Cartaya, "An Analytical and Experimental Investigation of the Stirling Cycle," Ph.D. Thesis, Mass. Inst. Technol., 1969.

9. W. R. Martini, "A Simple Method of Calculating Stirling Engines for Design Optimization," Thirteenth Intersociety Energy Conversion Engineering Conference Proceedings, Vol. 3. Warrendale, Pa., Society of Automotive Engineers, Inc., 1978, pp. 1753-1762.

10. A Collection of Stirling Engine Reports from General Motors Research, 1958-1970. Research Publication GMR-2690 (Publication arranged by NASA Lewis with permission from General Motors Research Labs., available from NTIS), 1978.

11. J. E. Cairelli, L. G. Thieme, and R. J. Walter, "Initial Test Results with a Single-Cylinder Rhombic-Drive Stirling Engine," DOE/NASA/1040-78/1, NASA TM-78919, July 1978.

12. L. G. Thieme and R. C. Tew, "Baseline Performance of the GPU-3 Stirling Engine," NASA TM-79038, 1978 (presented at DOE Highway Vehicle Systems Contractors Coordination Meeting, Dearborn, Mich., October 17-20, 1978).

13. W. H. Percival, "Historical Review of Stirling Engine Development in the United States from 1960 to 1970. Rept. 4-E8-00595, General Motors Research Labs., ERDA Contract EPA-4-E8-00595, NASA CR-121097, July 1974.

14. W. M. Kays and A. L. London, "Compact Heat Exchangers," Second ed., New York, N.Y.: McGraw Hill Book Co., Inc., 1964.

15. W. H. McAdams, "Heat Transmission," Third ed., New York, N.Y.: McGraw Hill Book Co., Inc., 1954.

Table 1 - GPU 3-2 Engine Dimensions and Parameters

Cylinder bore at liner, cm (in.)	6.99 (2.751)
Cylinder bore above liner,* cm (in.)	7.01 (2.76)
Cooler	
Tube length, cm (in.)	4.61 (1.813)
Heat transfer length, cm (in.)	3.55 (1.399)
Tube inside diameter, cm (in.)	0.108 (0.0425)
Tube outside diameter, cm (in.)	0.159 (0.0625)
Number of tubes per cylinder (or number of tubes per regenerator)	312 (39)
Heater	
Mean tube length, cm (in.)	24.53 (9.658)
Heat transfer length, cm (in.)	15.54 (6.12)
Cylinder tube, cm (in.)	11.64 (4.583)
Regenerator tube, cm (in.)	12.89 (5.075)
Tube inside diameter, cm (in.)	0.302 (0.119)
Tube outside diameter, cm (in.)	0.483 (0.19)
Number of tubes per cylinder (or number of tubes per regenerator)	40 (5)
Cold end connecting ducts	
Length, cm (in.)	1.59 (0.625)
Duct inside diameter, cm (in.)	0.597 (0.235)
Number of ducts per cylinder	8
Cooler end cap, cm^3 (in^3)	0.279 (0.0170)
Regenerators	
Length (inside), cm (in.)	2.26 (0.89)
Diameter (inside), cm (in.)	2.26 (0.89)
Number per cylinder	8
Material	Stainless steel wire cloth
Number of wires, per cm (per in.)	79×79 (200×200)
Wire diameter, cm (in.)	0.004 (0.0016)
Number of layers	308
Filler factor, percent	30.3
Angle of rotation between adjacent screens, deg	5
Drive	
Connecting rod length, cm (in.)	4.60 (1.810)
Crank - radius, cm (in.)	1.38 (0.543)
Eccentricity, cm (in.)	2.08 (0.820)
Miscellaneous	
Displacer rod diameter, cm (in.)	0.952 (0.375)
Piston rod diameter, cm (in.)	2.22 (0.875)
Displacer diameter, cm (in.)	6.96 (2.740)
Displacer wall thickness, cm (in.)	0.159 (0.0625)
Displacer stroke, cm (in.)	3.12 (1.23)
Expansion space clearance, cm (in.)	0.163 (0.064)
Compression space clearance, cm (in.)	0.030 (0.012)
Buffer space maximum volume, cm^3 (in^3)	521 (31.78)
Total working space minimum volume, cm (in)	233.5 (14.25)

*Top of displacer seal is at top of liner at displacer TDC.

Table 2 - GPU-3 Stirling Engine Dead Volumes

[Volumes are given in cu cm (cu in.)]

I. Expansion space clearance volume	
Displacer clearance (around displacer)	3.34 (0.204)
Clearance volume above displacer	7.41 (0.452)
Volume from end of heater tubes into cylinder	1.74 (0.106)
Total	12.5 (0.762)
II. Heater dead volume	
Insulated portion of heater tubes next to expansion space	9.68 (0.591)
Heated portion of heater tubes	47.46 (2.896)
Insulated portion of heater tubes next to regenerator	13.29 (0.811)
Additional volume in four heater tubes used for instrumentation	2.74 (0.167)
Volume in header	7.67 (0.468)
Total	80.8 (4.933)
III. Regenerator dead volume	
Entrance volume into regenerators	7.36 (0.449)
Volume within matrix and retaining disks	53.4 (3.258)
Volume between regenerators and coolers	2.59 (0.158)
Volume in snap ring grooves at end of coolers	2.18 (0.133)
Total	65.5 (3.998)
IV. Cooler dead volume	
Volume in cooler tubes	13.13 (0.801)
V. Compression in space clearance volume	
Exit volume from cooler	3.92 (0.239)
Volume in cooler end caps	2.77 (0.169)
Volume in cold end connecting ducts	3.56 (0.217)
Power piston clearance (around power piston)	7.29 (0.445)
Clearance volume between displacer and power piston	1.14 (0.070)
Volume at connections to cooler end caps	2.33 (0.142)
Volume in piston "notches"	0.06 (0.004)
Volume around rod in bottom of displacer	0.11 (0.007)
Total	21.18 (1.293)
Total dead volume	193.15 (11.787)
Minimum live volume	39.18 (2.391)
Calculated minimum total working space Volume	232.3 (14.178)
Measured value of minimum total working space volume (by volume displacement)	233.5 (14.25)
Change in working space volume due to minor engine modification	2.5 (0.15)
	236.0 (14.40)

Table 3 - Summary of Comparisons Between Predicted and Experimental Brake Power and Efficiency

Working gas	Heater gas temperature, °C (°F)	Performance parameter	Mean pressure, N/m^2 (psi)	Percent or absolute value of predicted performance parameter relative to experimental value
Hydrogen	704 (1300)	Power	4.14×10^6 (600) and 2.76×10^6 (400)	0 to 6 percent above
			1.38×10^6 (200)	0.07 kW (0.1 hp) to 0.22 kW (0.3 hp) above
		Efficiency	4.14×10^6 (600)	7 percent above upper experimental value
			2.76×10^6 (400)	6 to 16 percent above upper experimental value
			1.38×10^6 (200)	6 to 30 percent above upper experimental value
Helium	649 (1200)	Power	6.90×10^6 (1000) to 2.76×10^6 (400)	2 to 15 percent above (except for lowest power point)
		Efficiency	6.90×10^6 (1000) to 2.76×10^6 (400)	3 to 17 percent above upper experimental value (except for lowest efficiency point)
	704 (1300)	Power	5.52×10^6 (800)	7 to 10 percent above
			4.14×10^6 (600) and 2.76×10^6 (400)	7 to 34 percent above

Table 4 - Leakage Losses for Hydrogen and Helium

Mean pressure, N/m^2 (psi)	Hydrogen loss, kW (hp)	Helium loss, kW (hp)
6.90×10^6 (1000)	0.45 (0.60)	0.31 (0.42)
5.52×10^6 (800)	0.28 (0.38)	0.20 (0.27)
4.14×10^6 (600)	0.16 (0.22)	0.12 (0.16)
2.76×10^6 (400)	0.07 (0.10)	0.05 (0.07)
1.38×10^6 (200)	0.015 (0.02)	0.007 (0.01)

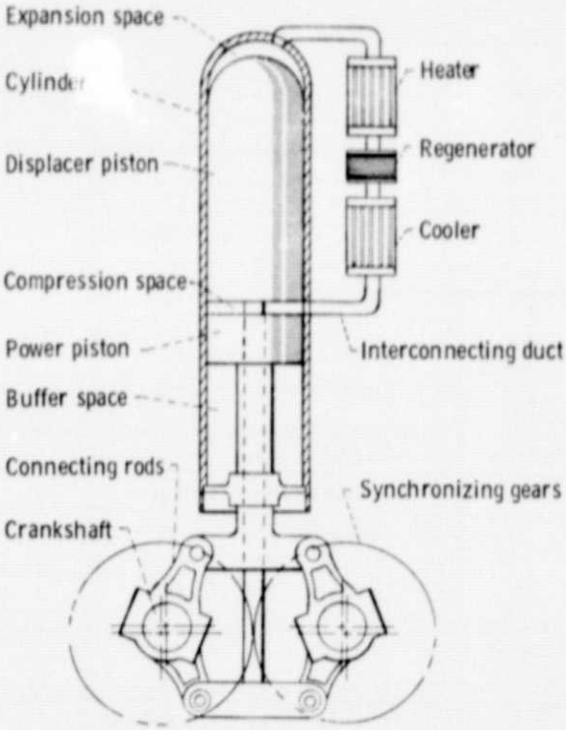

Figure 1. - Schematic of a single-cylinder Stirling engine with rhombic drive.

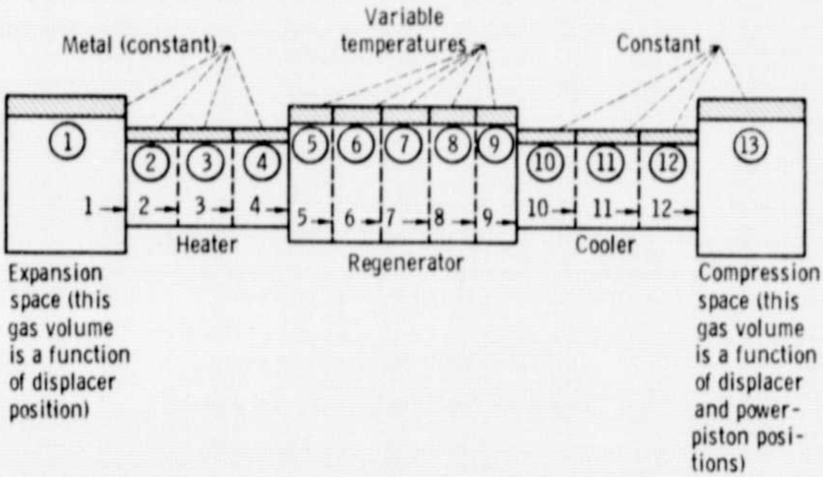

Figure 2. - Heat- and mass-transfer control volumes.

E-9040

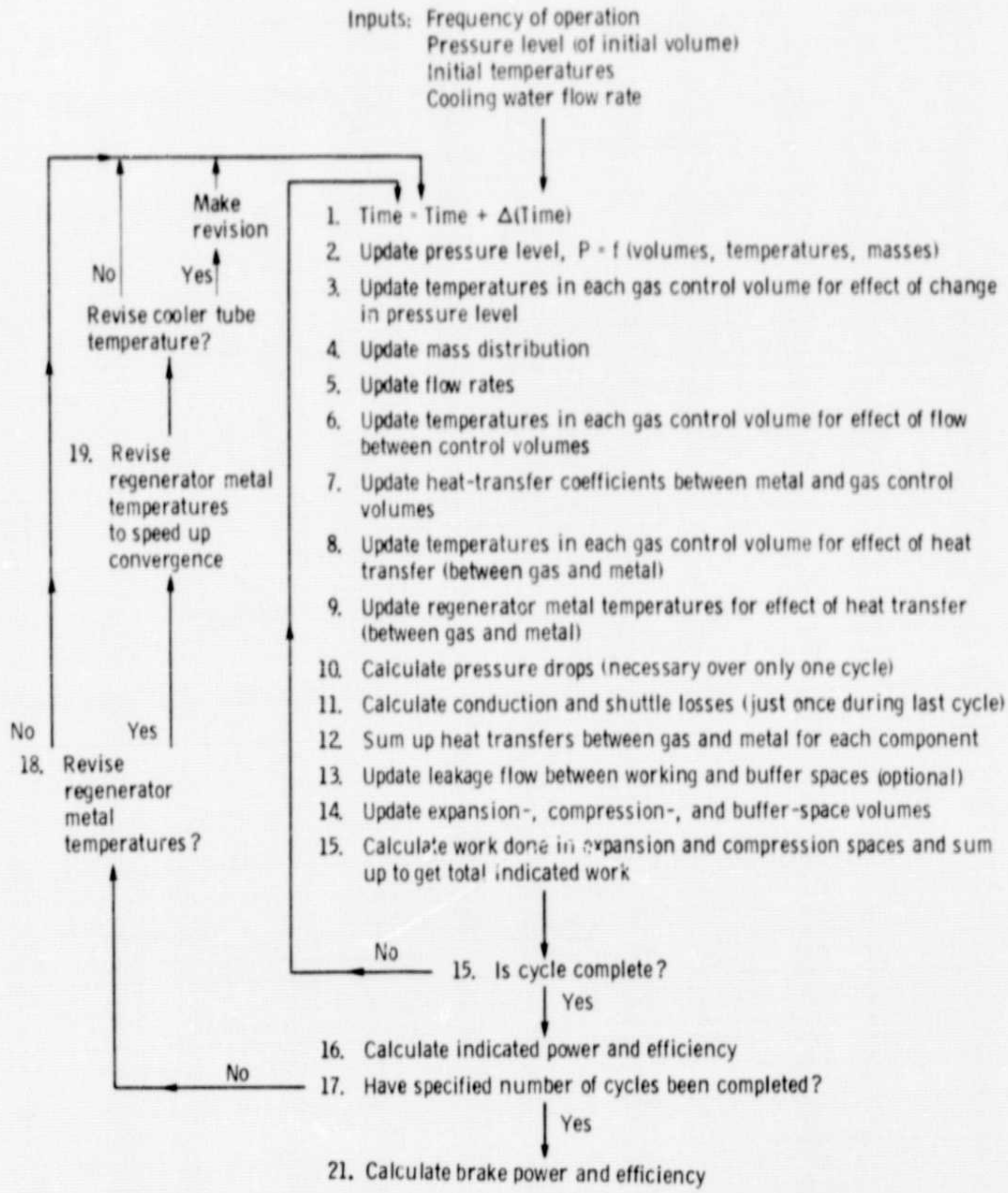

Figure 3. - Outline of calculation procedure.

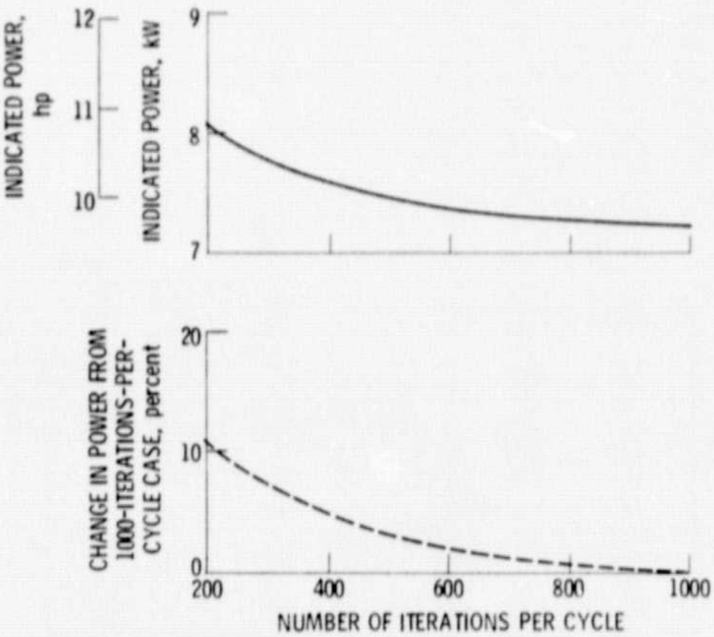

Figure 4. - Indicated power and change in indicated power as function of number of iterations per cycle. Working fluid, helium; frequency, 50 hertz; heater-tube temperature, 978 K (1760° R); cooler-tube temperature, 325 K (585° R); mean pressure, 4.43×10^6 N/m^2 (643 psi).

E-9848

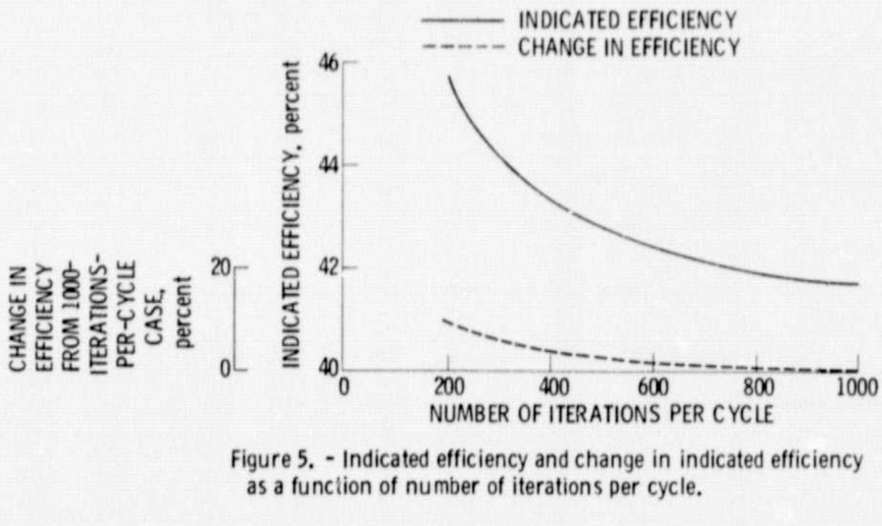

Figure 5. - Indicated efficiency and change in indicated efficiency as a function of number of iterations per cycle.

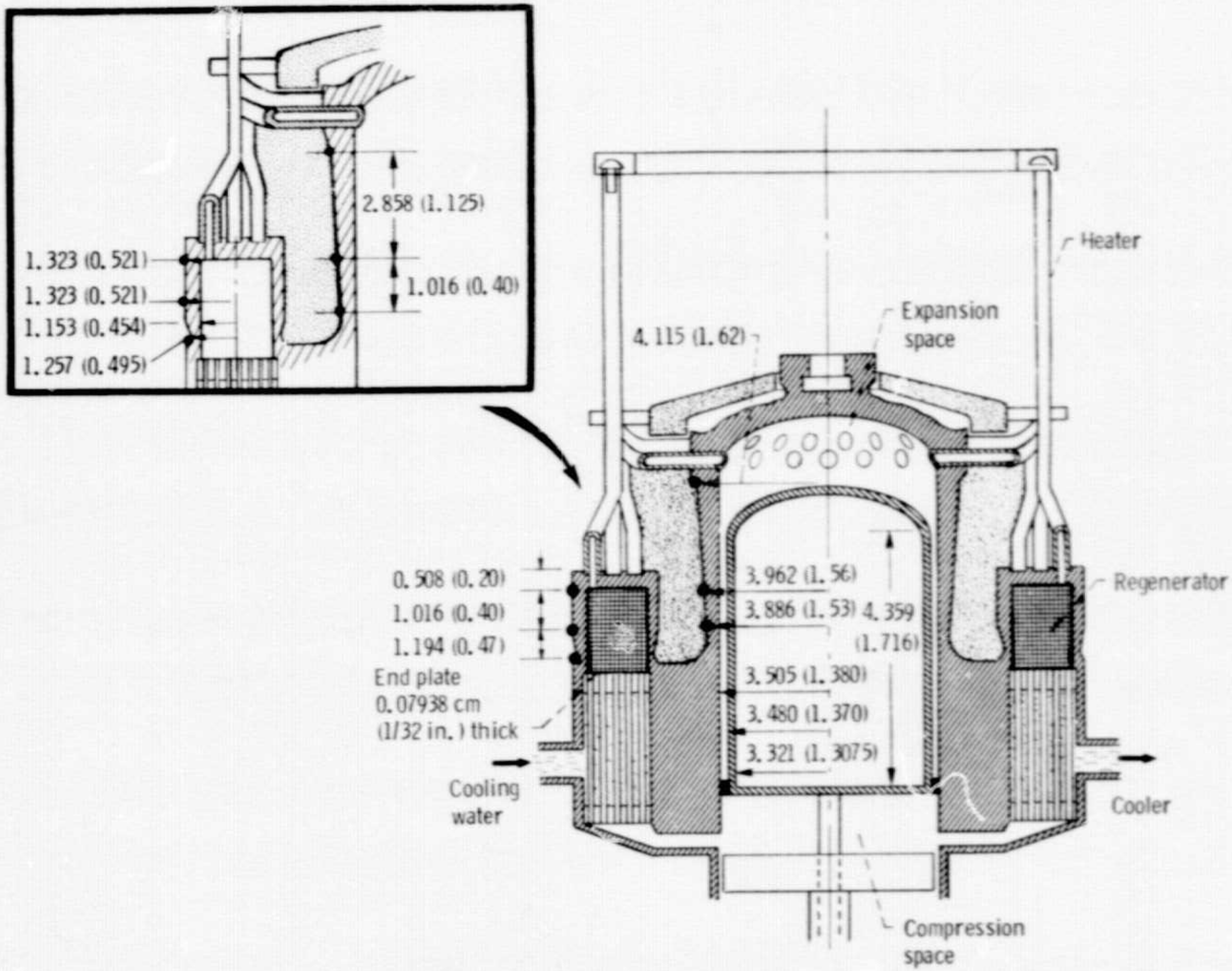

Figure 6. - Schematic showing dimensions needed for calculating heat conduction. (Regenerator, housing, cylinder, and displacer are 310 stainless steel. Dimensions are in cm (in.).)

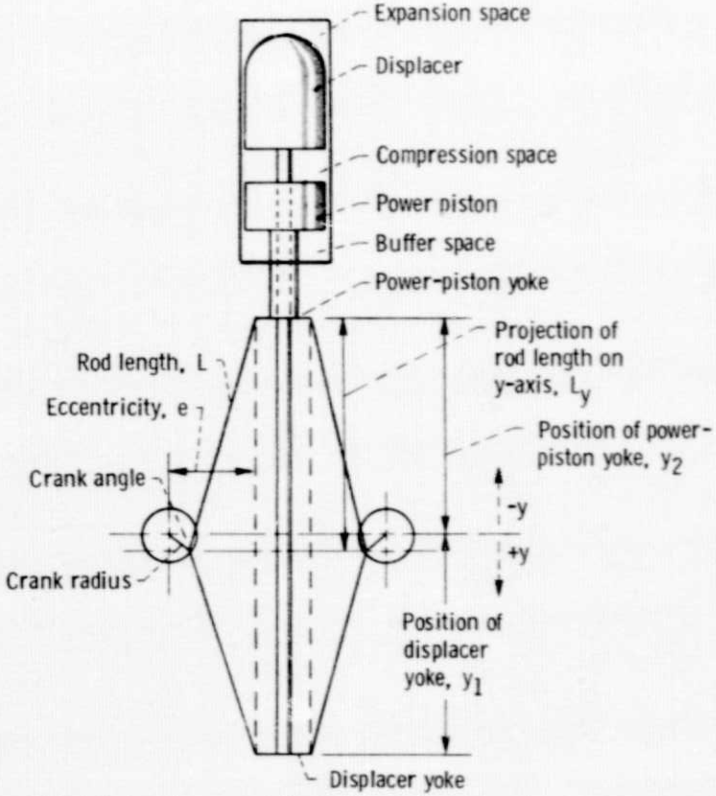

Figure 7. - Schematic showing geometric relations between piston positions and crankshaft angle.

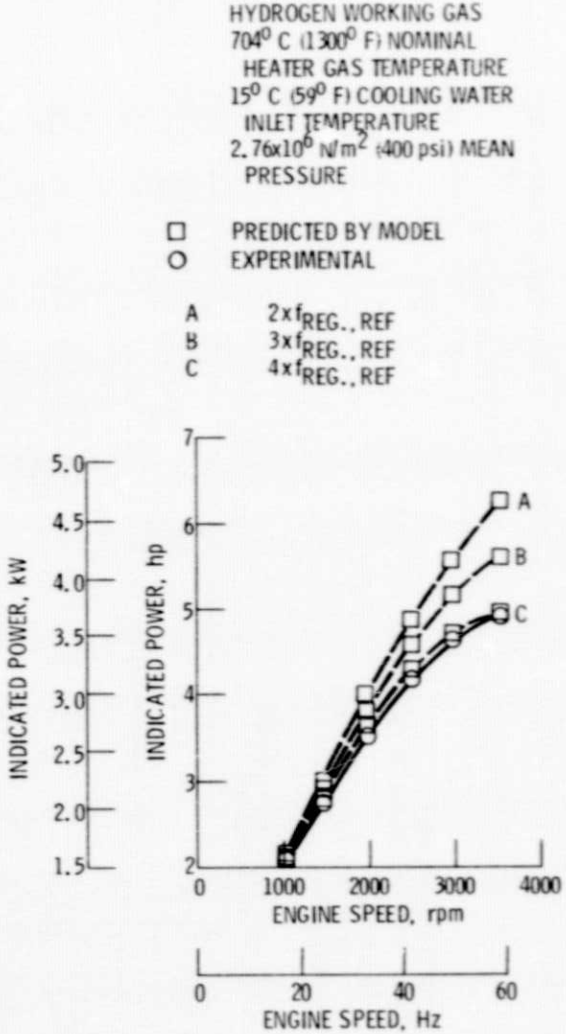

Figure 8. - Effect of regenerator friction factor, $f_{REG.}$, on predicted indicated power.

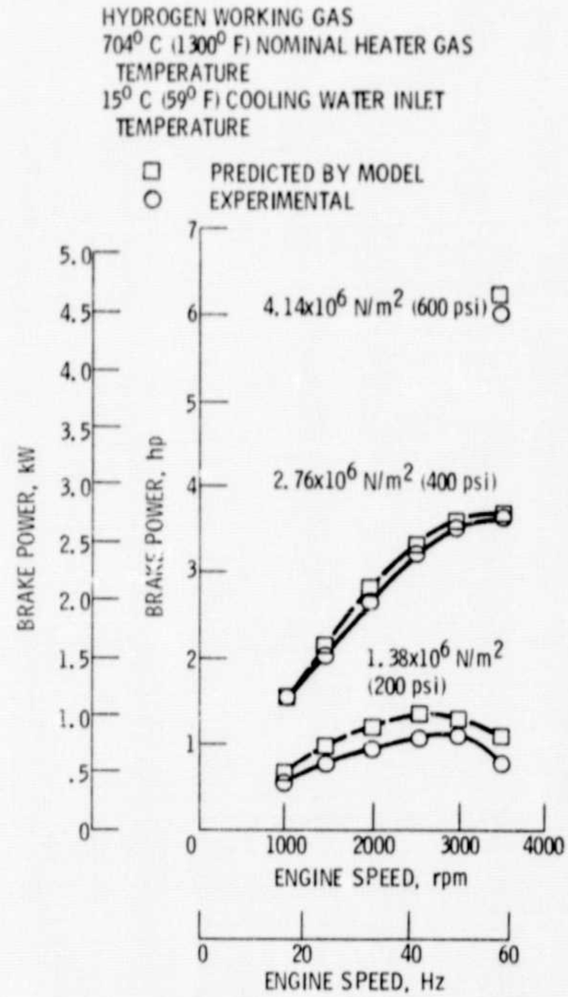

Figure 9. - Brake power as a function of engine speed at several mean pressures.

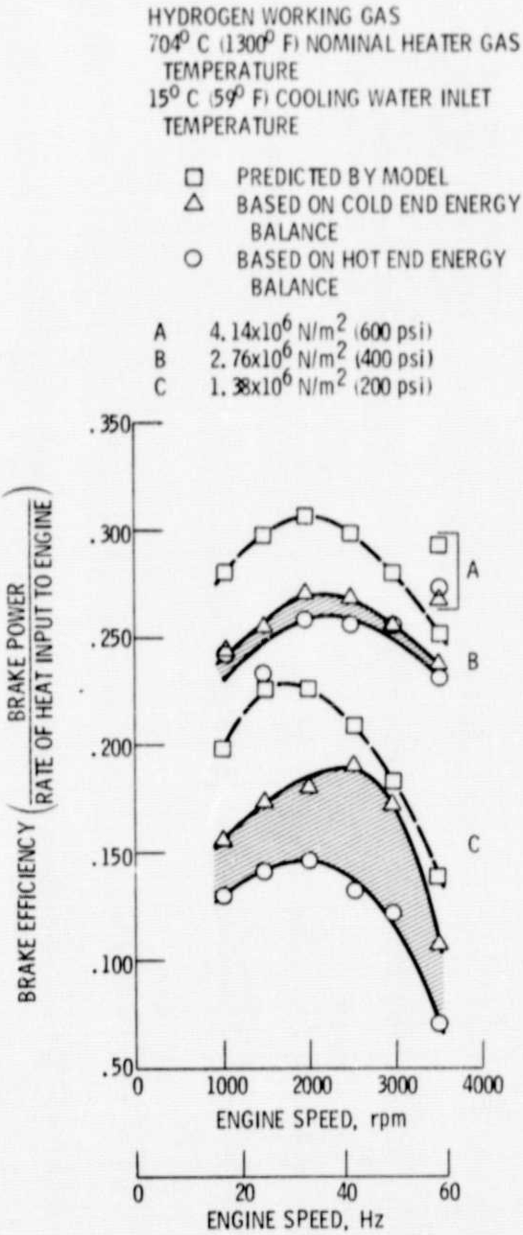

Figure 10. - Brake efficiency as a function of engine speed at several mean pressures.

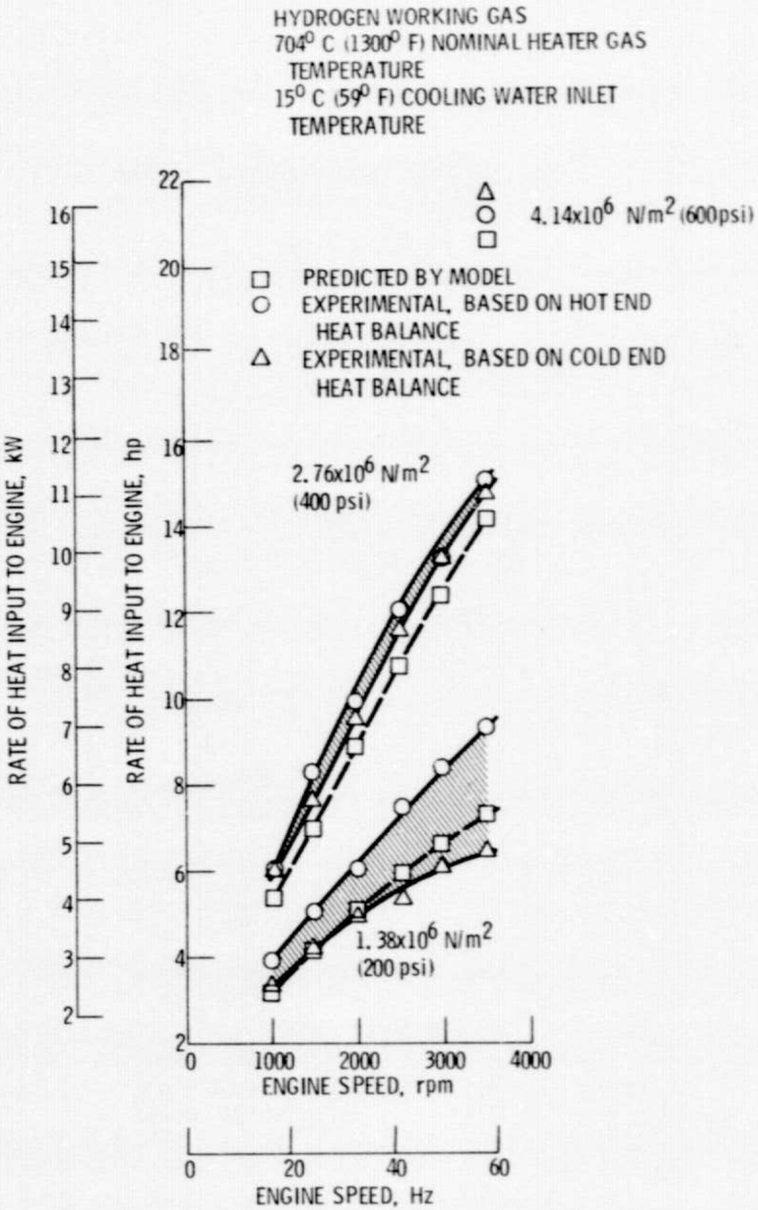

Figure 11. - Rate of heat input as a function of engine speed.

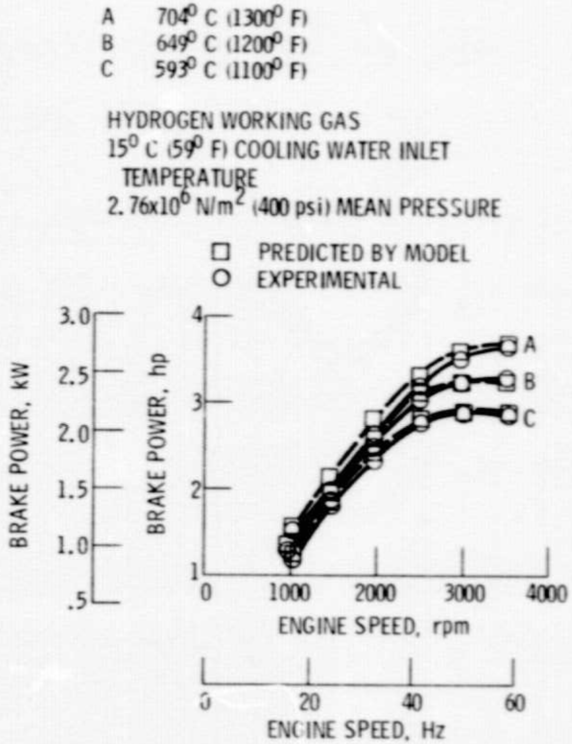

Figure 12. - Brake power as a function of speed at three different heater gas temperatures.

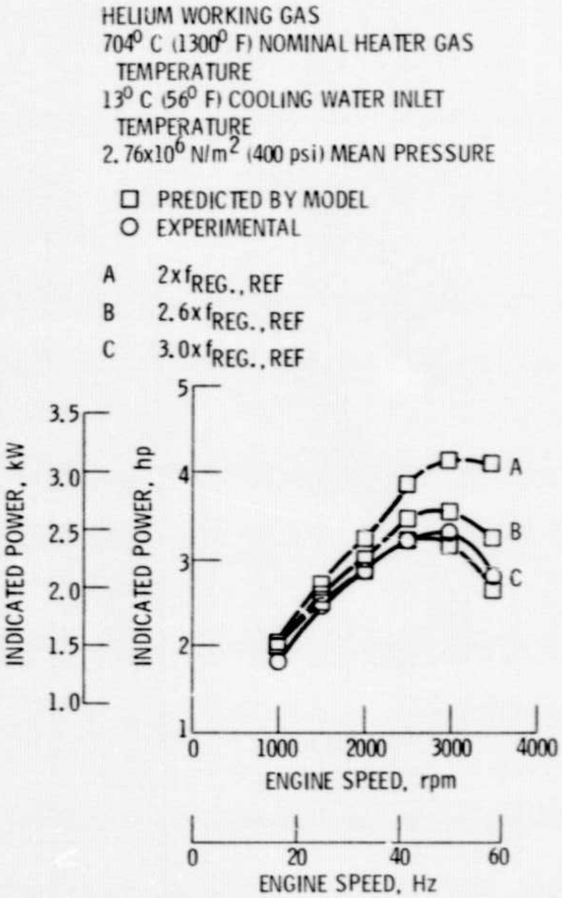

Figure 13. - Effect of regenerator friction factor, $f_{REG.}$, on predicted indicated power.

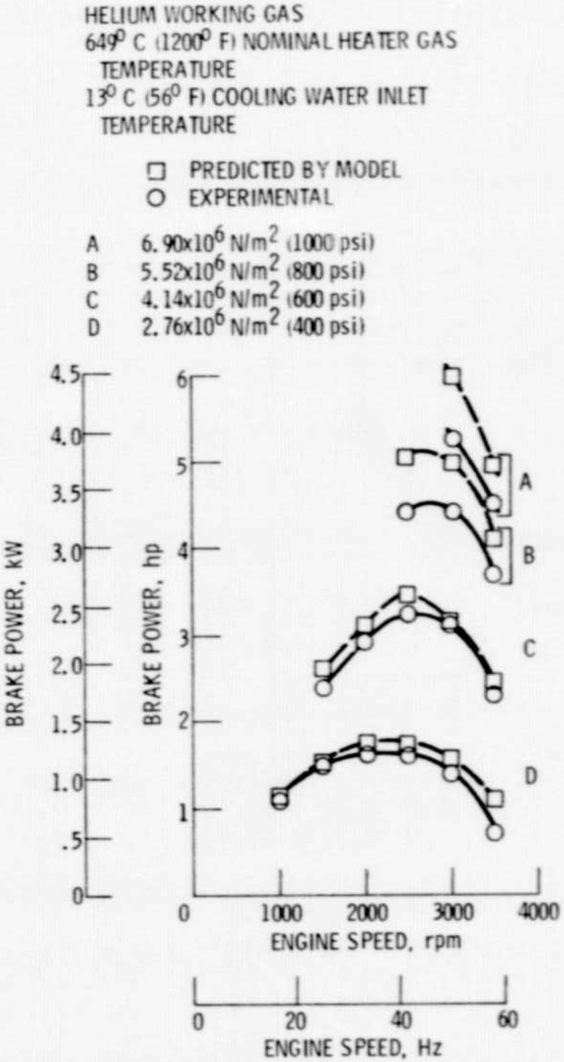

Figure 14. - Brake power as a function of engine speed at several mean pressures.

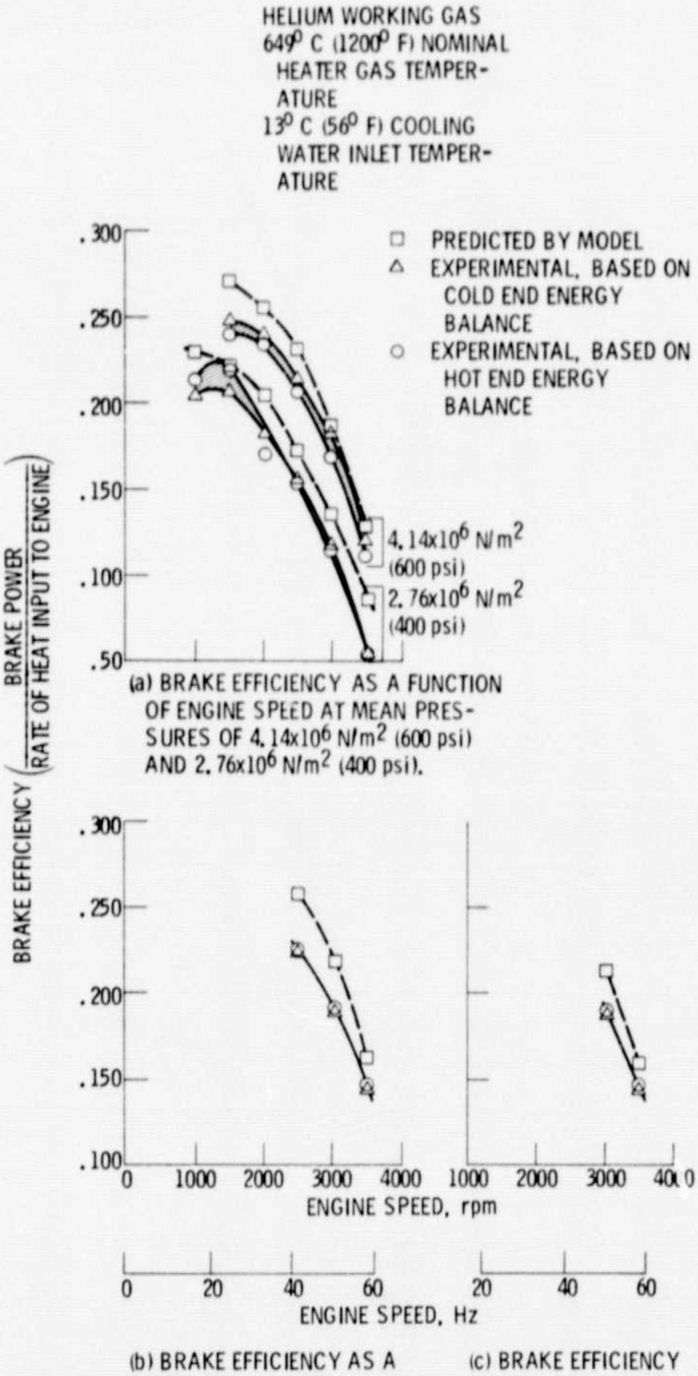

(a) BRAKE EFFICIENCY AS A FUNCTION OF ENGINE SPEED AT MEAN PRESSURES OF 4.14×10^6 N/m^2 (600 psi) AND 2.76×10^6 N/m^2 (400 psi).

(b) BRAKE EFFICIENCY AS A FUNCTION OF ENGINE SPEED AT A MEAN PRESSURE OF 5.52×10^6 N/m^2 (800 psi).

(c) BRAKE EFFICIENCY AS A FUNCTION OF ENGINE SPEED AT A MEAN PRESSURE OF 6.90×10^6 N/m^2 (1000 psi).

Figure 15.

E-9048

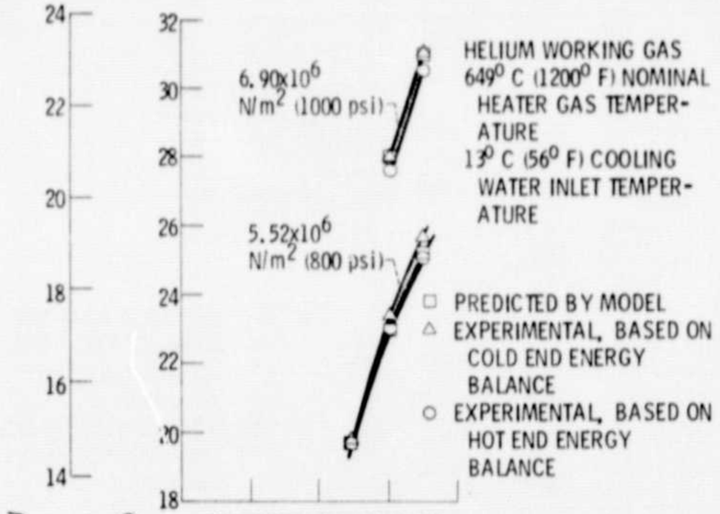

(a) RATE OF HEAT INPUT TO ENGINE AS A FUNCTION OF ENGINE SPEED AT MEAN PRESSURES OF 6.90×10^6 N/m^2 (1000 psi) AND 5.52×10^6 N/m^2 (800 psi).

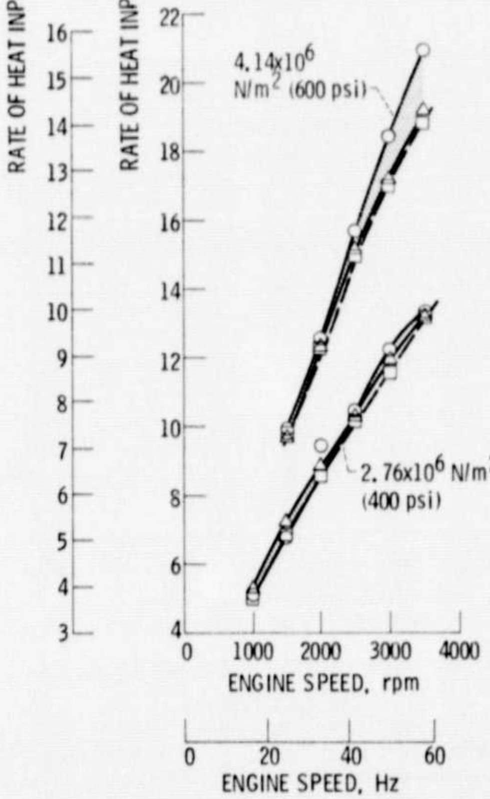

(b) RATE OF HEAT INPUT TO ENGINE AS A FUNCTION OF ENGINE SPEED AT MEAN PRESSURES OF 4.14×10^6 N/m^2 (600 psi) AND 2.76×10^6 N/m^2 (400 psi).

Figure 16.

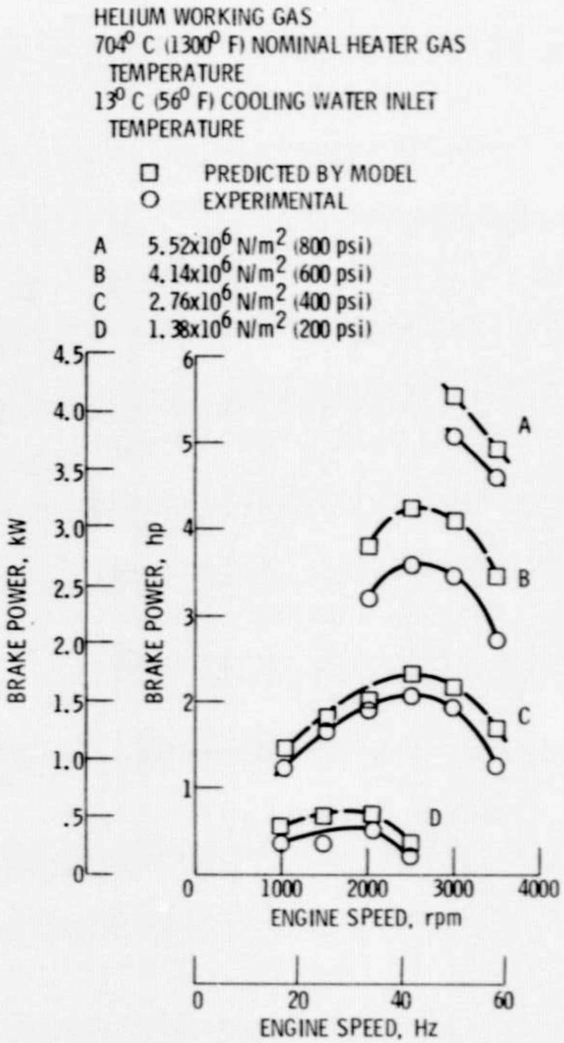

Figure 17. - Brake power as a function of engine speed at several mean pressures.

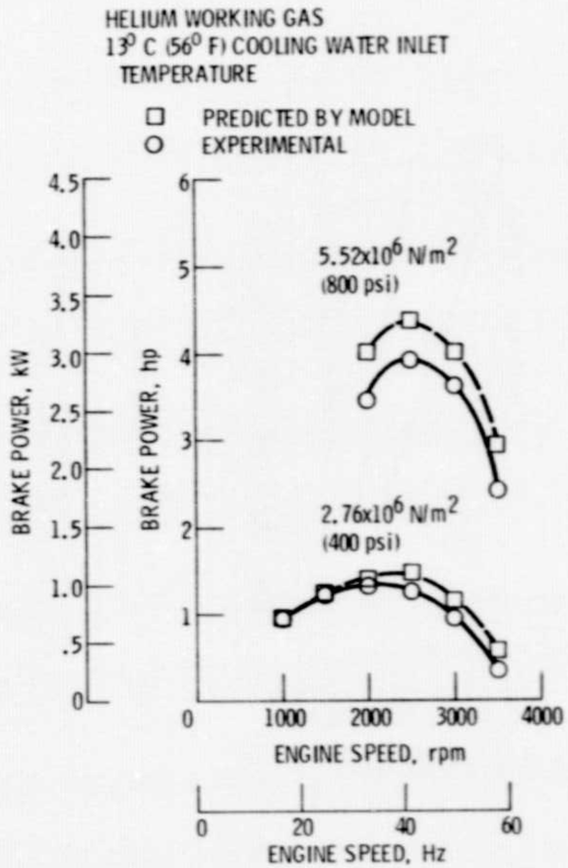

Figure 18. - Brake power as a function of engine speed at 593° C (1100° F) nominal heater gas temperature.

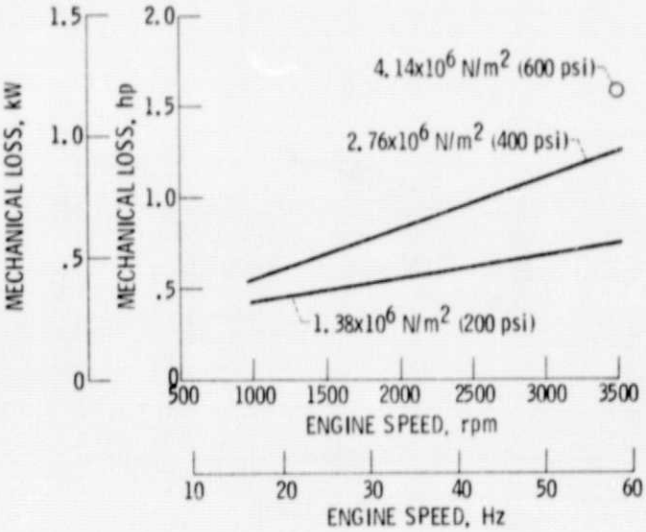

Figure 19. - Mechanical loss as a function of engine speed for hydrogen working gas. (Determined from experimental heat balance.)

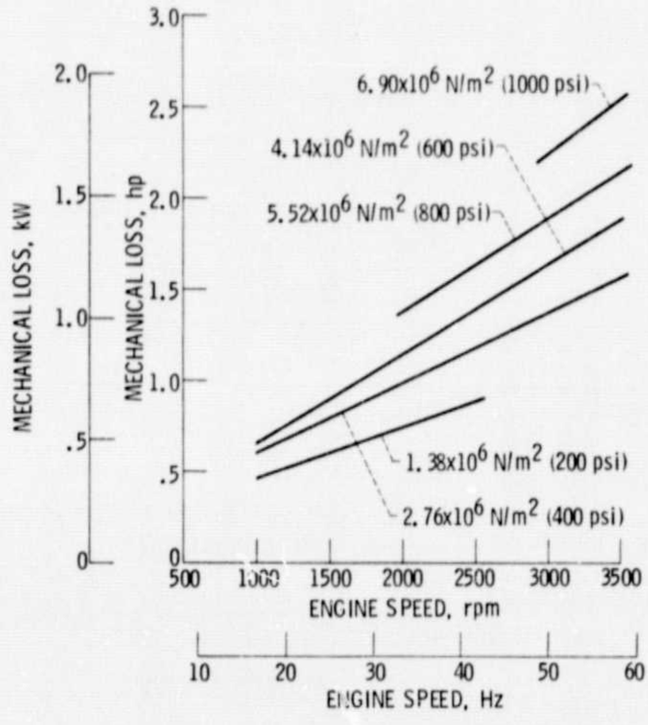

Figure 20. - Mechanical loss as a function of engine speed for helium working gas. (Determined from experimental heat balance.)

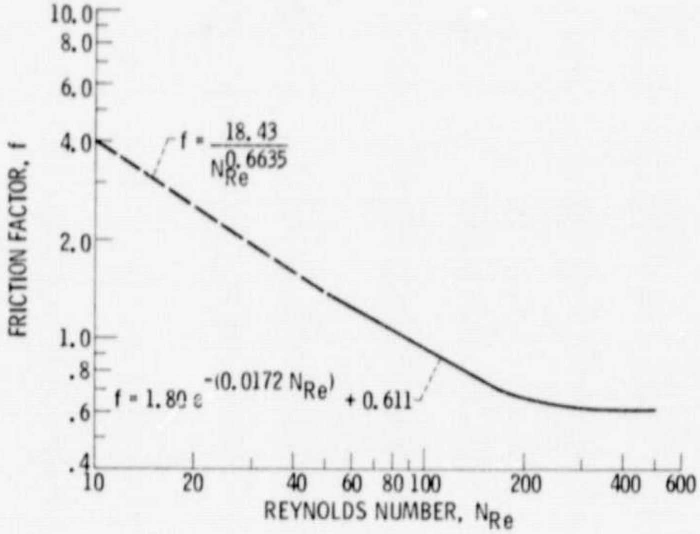

Figure 21. - Regenerator friction factor, f as a function of Reynolds number, N_{Re}.

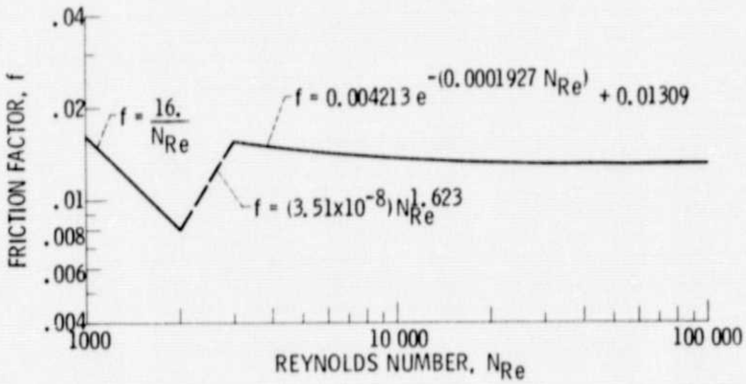

Figure 22. - Cooler friction factor, f, as a function of Reynolds number, N_{Re}.